JURNAL KARTIKA KIMIA

J. Kartika Kimia, May 2025, 8, (1), 129-141
Journal homepage: http://jkk.unjani.ac.id/index.php/jkk
P-ISSN: 2655-1322 E-ISSN: 2655-0938

Density Functional Theory Investigation of NO_2 Gas Adsorption Properties on $X_{12}Y_{12}$ Nanocages (X= B, In and Y = As, P)

Atthar Luqman Ivansyah[1,*], Riska Cindi Yustiarini[2], Jamal Abdul Nasir[3], and Tety Sudiarti[2]
[1]Physical and Inorganic Chemistry Division, Department of Chemistry, Faculty of Mathematics and Natural Sciences, Institut Teknologi Bandung, Bandung 40132, Indonesia
[2]Department of Chemistry, Faculty of Science and Technology, UIN Sunan Gunung Djati, Bandung 40614, Indonesia
[3]Department of Chemistry, Kathleen Lonsdale Materials Chemistry University College London, 20 Gordon Street, London WC1H 0AJ, United Kingdom
*E-mail: atthar@csx.itb.ac.id

DOI: https://doi.org/10.26874/jkk.v8i1.935

Received: 12 May 2025, *Revised*: 3 July 2025, *Accepted*: 4 July 2025, O*nline*: 5 July 2025

Abstract

This study investigates the structural, electronic, and physical properties of $X_{12}Y_{12}$ (X = B, In, and Y = As, P) fullerene-like cages for NO_2 adsorption. We employ Density Functional Theory (DFT) calculations with B3LYP methods, LANL2DZ basis set, and D4 dispersion correction to explore these properties, including ionization potential and electronic affinity linked to HOMO-LUMO gap energy. Moreover, this study explores global reactivity indices such as chemical potential, ionization potential, hardness, and softness. It also examines electronic properties, such as density of states (DOS), natural bond orbital (NBO), and electrostatic potential (ESP), along with chemical interactions like IGMH and AIMD, within the system. The findings demonstrate that the $B_{12}As_{12}$ nanocage exhibits high sensitivity to NO_2 molecules, as evidenced by the bond interaction and adsorption energy of -273.33 kJ/mol, supported by UV-vis and IRI graphics, with the order of systems from the lowest to the highest adsorption energy toward NO_2 : $B_{12}P_{12}$-NO_2 < $In_{12}As_{12}$-NO_2 < $In_{12}P_{12}$-NO_2 < $B_{12}As_{12}$-NO_2. AIMD simulations indicate that all nanocages can effectively adsorb NO_2 within varying lengths by 1000 fs. This suggests the potential for high NO_2 gas adsorption by the $B_{12}As_{12}$ nanocage. Further investigation is required to assess the potential of other nanocages.

Keywords: Adsorption, Density functional theory, Nanocage, Nitrogen dioxide

1 Introduction

The growing awareness of the negative effects of environmental pollution on human health and ecosystem integrity has highlighted the need for sustainable solutions to reduce air pollutants. One such pollutant is nitrogen dioxide (NO_2), which is a toxic gas produced by the combustion of fossil fuels and is a significant contributor to air pollution. The World Health Organization (WHO) has also identified NO_2 as a toxic gas and a major contributor to air pollution, primarily originating from human activities such as vehicle emissions, industrial processes, and combustion processes [1] [2]. Owing to its potential health risks, including respiratory ailments, cardiovascular diseases, environmental degradation, increased economic burdens, and mortality [1][2][3][4][5], there is a need for effective gas adsorption materials to remove NO_2 from the atmosphere.

Inorganic fullerene-like nanocages exhibit distinctive electrical and mechanical properties [6]. Following the discovery of H.W Kroto and his team in 1985, a new material, C_{60} or fullerene, was identified [7]. This material, known as a nanocluster or nanocage, is nearly spherical and stable. Nanocages are materials with a hollow structure that can trap and store gas molecules within their cavity. Gas molecules adsorbed onto the nanocage surface can result in the formation of a single or multiple layer, depending on the adsorption energy and the characteristics of the gas molecules and nanocages. According to a study conducted by Xu et al. in 2006, the most stable nanocluster or nanocage (XY) was identified, featuring a value of 12 and cut-off octagonal shape consisting of eight hexagons and six squares [8].

Among the various nanocage materials, boron-based and indium-based cages, exemplified by $B_{12}As_{12}$, $B_{12}P_{12}$, $In_{12}As_{12}$, and $In_{12}P_{12}$, have gained significant attention due to their intriguing structural motifs and potential for gas adsorption studies. There have been few studies on nanocages constructed with boron, indium, phosphorus, and arsenic atoms. For instance, the adsorption of one oxygen atom on the boron atom of $B_{12}P_{12}$ nanocavity is stronger than other methods, as demonstrated by Karimi and Dashti [9]. On the other hand, the adsorption of CO_2 on a pure $B_{12}P_{12}$ nanocage yields one geometry with an adsorption energy of −4.88 kJ/mol, according to a study by Shahid Hussain, et al [10], which considered the nanocages as potential candidates for application in CO_2 gas sensors. Nanocage $B_{12}P_{12}$ reported in Behestian's research, et al. [11] reported that the electron density of adsorbing atoms plays a crucial role in the hydrogen gas adsorption on the $B_{12}P_{12}$. This adsorption is thermodynamically viable above the apexes of both boron and phosphorus atoms within the cluster, with Gibbs free energies of −1.18 and −0.80 eV, respectively [12]. Furthermore, a study by A. Ektarawong, et al. in 2017 [13] identified icosahedral $B_{12}As_{12}$ as the only stable compound in the binary B-As system.

The diverse range of structures and compositional versatility of these nanocages provide a rich platform for exploring their adsorption properties toward NO_2 gas molecules. The incorporation of heteroatoms, such as arsenic (As) and phosphorus (P), into boron (B) or indium (In) into these cages, creates distinct electronic characteristics, which can influence the interaction strength and binding affinity with NO_2 species. Furthermore, the inherent porosity and surface features of these nanocages play important roles in determining the adsorption kinetics and thermodynamics, necessitating a comprehensive investigation into their adsorption behaviour. The significance of this study lies in the potential applications for identifying the adsorption properties of NO_2 gas on $X_{12}Y_{12}$ (X = B, In and Y = As, P) nanocages. By investigating the properties of these nanocages, new materials can be developed for the removal of NO_2 gas from the environment to enhance air quality and promote human health. Quantum chemistry calculations were conducted using quantum mechanics and density functional theory to identify effective and potential nanocages for adsorbing nitrogen dioxide (NO_2) gas. Four types of $X_{12}Y_{12}$ (X = B, In and Y = As, P) nanocages were examined to identify the most effective and potential nanocages for adsorbing NO_2 gas. Electronic properties, adsorption energy, frontier molecular orbital (FMO) analysis, quantum theory of atoms in molecules (QTAIM), natural bonding orbital (NBO), total density of states (TDOS), independent gradient model based on Hirshfeld partition (IGMH), and electrostatic potential (ESP) analyses were conducted on $X_{12}Y_{12}$ nanocages to address the questions raised by the problem.

2 Method

In this study, the adsorption of NO_2 into the $X_{12}Y_{12}$ (X = B, In and Y = As, P) nanocages was theoretically investigated using density functional theory (DFT) calculations conducted using the ORCA quantum chemistry program [14]. To improve the measurement of computational accuracy, the calculations employed the B3LYP (Becke gradient-corrected exchange functional and Lee−Yang−Parr correlation functional with three parameters) [15] level theory to improve the measurement of computational accuracy [16] [17] [18]. The LANL2DZ (Lot Alamos National Laboratory 2 Double ζ) [19] basis set with dispersion of D4 correction [20] was employed to optimize the geometry of $X_{12}Y_{12}$ (X = B, In and Y = As, P) nanocages with the convergence thresholds in geometry optimization are $\mathrm{TolE} = 5 \times 10^{-6}, \mathrm{TolRMSG} = 1 \times 10^{-4}, \mathrm{TolMaxG} = 3 \times 10^{-4}, \mathrm{TolRMSD} = 2 \times 10^{-3}$, and $\mathrm{TolMaxD} = 4 \times 10^{-3}$, which TolE (Energy) is the maximum allowed change in energy between optimization steps; TolRMSG (RMS Gradient) is the maximum allowed RMS gradient; TolMaxG (Maximum Gradient) is the maximum allowed component of the gradient; TolRMSD (RMS Displacement) is the maximum allowed RMS displacement of atoms between steps; and TolMaxD (Maximum Displacement) is the maximum allowed displacement of any single atom between steps. In calculations involving transition metals, an all-electron basis set is employed on the LANL2DZ basis set for all non-transition metal atoms. D4 correction was performed to accurately and self-consistently calculate the electronic energy to obtain the adsorption energy, enhance intermolecular interactions, and provide values that can be compared with experimental results and existing references to challenge the adsorption energies. The D4 model is an advanced version of the D3 model, providing a more precise method for calculating London dispersion interactions in DFT and other atomistic methods. DFT-D4 is a physically improved and more sophisticated dispersion model in place of DFT-D3 for DFT calculations as well as for other low-cost approaches like semi-empirical models [21]. To develop the model, all molecular structures of $X_{12}Y_{12}$ nanocages, including $B_{12}As_{12}$, $B_{12}P_{12}$, $In_{12}As_{12}$, and $In_{12}P_{12}$, were described using Avogadro software version 1.2.0 [22]. The resulting 3D molecular structures of the $X_{12}Y_{12}$ nanocages were Visualized, optimized, and characterized using the Chemcraft b610b package [23].

The adsorption energy, E_{ads} was calculated from the interactions between $X_{12}Y_{12}$ nanocages and the NO_2 gas were calculated as follows **Eq. 1**:

$$E_{ads} = E_{gas\text{-}nanocage} - (E_{gas} + E_{nanocage}) \qquad \text{(Equation 1)}$$

Here, $E_{gas\text{-}nanocage}$ corresponds to the adsorption energy of the nanocage for gas, E_{gas} represents the energy of the isolated NO_2 gas, the pure nanocage is denoted by, and $E_{nanocage}$ is the energy term of the adsorbent, i.e., $B_{12}As_{12}$, $B_{12}P_{12}$, $In_{12}As_{12}$, and $In_{12}P_{12}$ nanocage cluster.

The specific properties of a molecule's structure and reactivity were analyzed through geometric optimization. This process involves examining reactivity through Frontier Molecular Orbital (FMO) analysis, thermodynamic properties, and intermolecular interactions. Frontier Molecular Orbital (FMO) analysis is used to understand the electronic structure of a molecule, particularly in relation to its activity. The ORCA quantum chemistry package is employed to examine the HOMO-LUMO states. Thermodynamic properties, such as Gibbs Energy (G), Enthalpy (H), and Entropy (S), were used to analyze the stability and energy changes that occur during chemical reactions at 298 K. These properties calculated using the following **Eq. 2 – 4**:

$$\Delta G = G_{gas\text{-}nanocage} - (G_{gas} + G_{nanocage}) \qquad \text{(Equation 2)}$$

$$\Delta H = H_{gas\text{-}nanocage} - (H_{gas} + H_{nanocage}) \qquad \text{(Equation 3)}$$

$$\Delta S = S_{gas\text{-}nanocage} - (S_{gas} + S_{nanocage}) \qquad \text{(Equation 4)}$$

The ionization potential (IP) and electron affinity (EA) are associated with the highest occupied molecular orbital (HOMO) and the lowest unoccupied molecular orbital (LUMO). This approach, known as orbital theory, is based on Koopmann's theory and provides a framework for calculating the stability of gas-nanocage systems. The stability can be calculated using **Eq. 5**:

$$\mu = \frac{E_{HOMO} + E_{LUMO}}{2} \qquad \text{(Equation 5)}$$

Various parameters are identified to comprehensively analyze the stability of gas-nanocage molecular systems, such as the energy gap between the lowest unoccupied molecular orbital (LUMO) and the highest occupied molecular orbital (HOMO) (E_{gap}), electrophilicity (ω), chemical potential (η), and softness (S). These parameters provide valuable insights into the electronic structure and reactivity of the system. The **Eq. 6 – 9** related to these parameters are as follows:

$$E_{gap} = E_{LUMO} + E_{HOMO} \qquad \text{(Equation 6)}$$

$$\omega = \frac{\mu^2}{2\eta} \qquad \text{(Equation 7)}$$

$$\eta = \frac{E_{LUMO} - E_{HOMO}}{2} \qquad \text{(Equation 8)}$$

$$S = \frac{1}{2}\eta \qquad \text{(Equation 9)}$$

Quantum theory analysis of atoms in the molecule (QTAIM) topological analysis and total partial densities of state (TDOS + PDOS), as well as the analysis of wavelength shifts in the UV-Vis spectrum, were evaluated using the Multiwfn software package version 3.8 [24]. UV-Vis analysis was used to determine the wavelength shift of the pure nanocage and after NO_2 adsorption. The chemical interactions within the molecules are represented by IGMH analysis. The molecular electrostatic potential (ESP) was also calculated using the multiwfn software version 3.8 [24], and the generated files were then exported to the VMD 1.9.1 [25] software for visualization purposes. The AIMD simulation was conducted at a temperature of 298.15 K with a Berendsen thermostat and the theory level of the B3LYP/LANL2DZ basis set, and D4 dispersion correction, from 0 to 5000 fs. The most stable orientation was determined from the final geometry of each system after 5000 fs.

3 Results and Discussion

3.1 Structural Properties

Nanocages play a crucial role in gas molecule adsorption. As illustrated in **Fig. 1**, these optimized structures comprise $B_{12}As_{12}$, $B_{12}P_{12}$, $In_{12}As_{12}$, and $In_{12}P_{12}$, all of which are composed of six squares and eight hexagon rings. All the atom sites on nanocages are identical [26]. NO_2, or nitrogen dioxide, is a reddish-brown gas with a pungent, were adsorbed onto nanocages to determine the most suitable adsorption sites. Furthermore, it was used to ascertain the interaction distance and adsorption energy in order to determine the optimal level of interaction [27]. Nitrogen Dioxide (NO_2) was adsorbed by four nanocages. This resulted in the formation of $B_{12}As_{12}$-NO_2, $B_{12}P_{12}$-NO_2, $In_{12}As_{12}$-NO_2, and $In_{12}P_{12}$-NO_2 as demonstrated in.

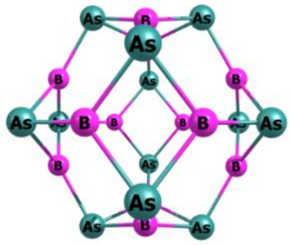

(a)

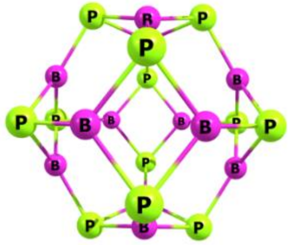

(b)

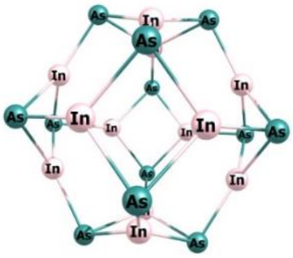

(c)

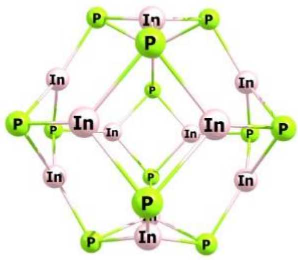

(d)

Figure 1 Geometry optimized for (a) $B_{12}As_{12}$, (b) $B_{12}P_{12}$, (c) $In_{12}As_{12}$, and (d) $In_{12}P_{12}$

Fig. 2 shows the optimized geometries of four clusters of nanocages, with NO_2 molecules adsorbed onto them. The bond length between the NO_2 molecules and the nanocages is shown in the figure. This alignment suggests a vertical orientation or alignment between the NO_2 molecules and the $B_{12}As_{12}$-NO_2, $In_{12}As_{12}$-NO_2, and $In_{12}P_{12}$-NO_2 nanocages during this interaction. As indicated, the interaction between NO_2 and nanocages is stable, and the molecules are not easily disrupted and are held in place or bonded to the nanocages. **Table 1** shows that the interaction distances of $B_{12}As_{12}$, $B_{12}P_{12}$, $In_{12}As_{12}$, and $In_{12}P_{12}$ molecule consecutively are 1.457 Å, 2.816 Å, 2.003 Å, and 2.163 Å. The greatest bond length was noted between an atom of the $B_{12}P_{12}$ cluster and the N atom of NO_2, measuring 2.816 Å. In this instance, the shortest bond length is observed in the $B_{12}As_{12}$ system, measuring 1.457 Å between the B and O atoms of the NO_2 gas molecule, as shown in **Table 1**.

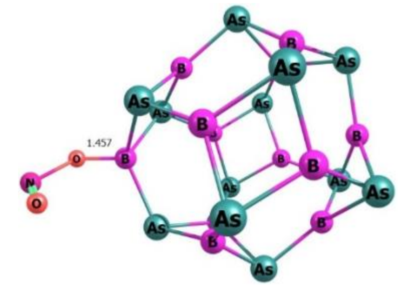

(a)

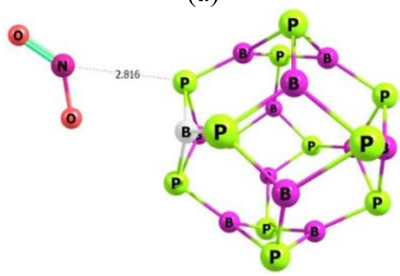

(b)

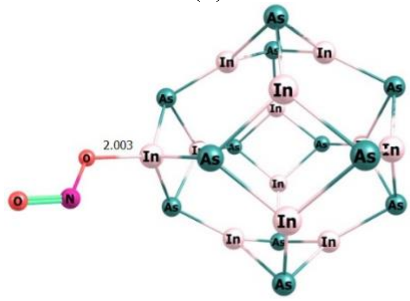

(c)

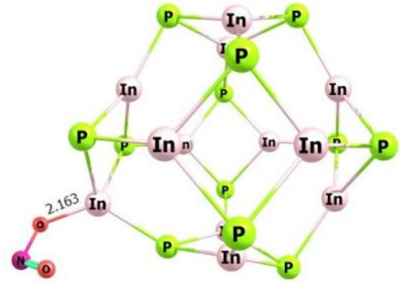

(d)

Figure 2 Distance between NO_2 and the nanocage (a) $B_{12}As_{12}$, (b) $B_{12}P_{12}$, (c) $In_{12}As_{12}$, and (d) $In_{12}P_{12}$

In the nanocages-NO_2 system, the order of interactions, from closest to farthest, was observed as follows: $B_{12}As_{12}$ < $In_{12}As_{12}$ < $In_{12}P_{12}$ < $B_{12}P_{12}$. Among these, $B_{12}As_{12}$ showed the most effective potential for adsorbing NO_2 molecule, as indicated by the computed data showing a more stable interaction on its surface [28]. $In_{12}As_{12}$ also can adsorb NO_2 molecule, being the second closest in distance among the systems studied. From that point, it indicates that nanocage systems with Y = As are potential adsorption agents for NO_2 based on their length distance. The structural characteristics regarding bond length were found to contrast with those of previous research [29]. The bond length values range from 2.01 Å to 3.42 Å for the $B_{12}P_{12}$ nanocages D1-D4 variations and CO_2 gases. In the case of previous research, the cluster $B_{12}P_{12}$ with CO_2 has a bond length of 3.42 Å [29]; however, it experiences a decrease in bond length upon the adsorption of NO_2 gas in $B_{12}P_{12}$.

Table 1 Distance between NO_2 and $X_{12}Y_{12}$ nanocage after geometry optimization

System	Distance (Å)
$B_{12}As_{12}$-NO_2	1.457
$B_{12}P_{12}$-NO_2	2.816
$In_{12}As_{12}$-NO_2	2.003
$In_{12}P_{12}$-NO_2	2.163

3.2 Adsorption Energy

The thermodynamic parameters of enthalpy change (ΔH) and Gibbs free energy (ΔG) are crucial indicators in adsorption processes. ΔG determines the spontaneity of the process. Simultaneously, ΔH provides valuable information about the interaction strength between gas molecules and the adsorbent material surface.

Table 2 Thermodynamic parameters of NO_2 adsorption on $X_{12}Y_{12}$ nanocage

System	E_{ads} (kJ/mol)	ΔG (kJ/mol)	ΔH (kJ/mol)
$B_{12}As_{12}$-NO_2	-273.3253	-103.876	-275.803
$B_{12}P_{12}$-NO_2	-126.7039	-31.5796	-129.184
$In_{12}As_{12}$-NO_2	-226.3418	-62.8988	-228.825
$In_{12}P_{12}$-NO_2	-258.2561	-91.9978	-260.732

Table 2 summarizes the adsorption energy value (ΔE) along with the thermodynamic parameters (ΔG and ΔH). **Table 2** shows that the value of the Gibbs free energy of all systems is negative except for $B_{12}P_{12}$. system. The negative value for ΔG indicates a spontaneous process of $B_{12}As_{12}$-NO_2, $In_{12}As_{12}$-NO_2, and $In_{12}P_{12}$-NO_2 adsorption system that the adsorption process is favorable and stability of three nanocage adsorption process [30]. Conversely, a positive Gibbs free energy value indicates a non-spontaneous process, suggesting that gas molecule adsorption on the surface is unlikely to occur without external intervention. The enthalpy energy values (ΔH) exhibit a negative trend. The negative sign of the enthalpy change indicates that the adsorption process is exothermic and energetically favorable. This suggests that the adsorption processes release heat and are generally exothermic. This aligns with the electron gain enthalpy concept, which is negative when energy is released upon accepting an electron. In the case of $B_{12}As_{12}$-NO_2, $In_{12}As_{12}$-NO_2, and $In_{12}P_{12}$-NO_2, chemical adsorption has drawbacks due to its tendency to release heat into the surrounding environment. The negative alterations in both enthalpies and Gibbs free energies signify that adsorption occurs spontaneously, resulting in heat release, suggesting a chemisorption mechanism. As emphasized in prior research, the process may vary depending on the characteristics of active sites and the coordination among atoms. Chemical adsorption has disadvantages because it releases heat into the environment. The negative changes in both enthalpies and Gibbs free energies indicate that adsorption occurs spontaneously, releasing heat, and suggesting a chemisorption process [31]. This process may vary depending on the characteristics of active sites and the coordination among atoms, as highlighted by previous studies [32]. Meanwhile, the adsorption energy (E_{ads}) value while NO_2 being adsorbed by $X_{12}Y_{12}$ nanocage surface. The increasing order of the adsorption energy of $X_{12}Y_{12}$-NO_2 system is $B_{12}P_{12}$-NO_2 (-126.7039 kJ/mol), $In_{12}As_{12}$-NO_2 (-226.3418 kJ/mol), $In_{12}P_{12}$-NO_2 (-258.2561 kJ/mol), and $B_{12}As_{12}$-NO_2 (-273.3253 kJ/mol). Based on the adsorption energy value and thermodynamic considerations, we categorize the process as chemisorption, which involves strong chemical bonds between the adsorbent and adsorbate, whereas physisorption involves weak van der Waals forces [33]. According to a standard guideline, if the adsorption energy is >50 kJ/mol, it is classified as chemisorption, and if it is 30 kJ/mol, it is classified as physisorption [34]. Higher adsorption energies indicate that the molecules are more strongly attracted to the surface, suggesting a stronger bond between the molecules and the surface. The E_{ads} value suggests that the E_{ads} system exhibits the lowest adsorption energy, indicating the strongest and most stable adsorption due to the superior ability of the adsorbent to attract adsorbate molecules. Consequently, the adsorption of NO_2 molecules on the surface of the $B_{12}As_{12}$ cluster is deemed more favourable for gas performance than other cluster nanocages.

3.3 *Frontier Molecular Orbital (FMO) Analysis*

A Frontier Molecular Orbital (FMO) study was used to analyse the properties and reactivity of the complete nanocage system. A detailed overview of quantum molecular computations is given in **Table S1**. The interaction between two molecules in a system can be analysed by determining the value of the highest occupied electron molecular orbital (HOMO) and the lowest unoccupied electron molecular orbital (LUMO), as well as the distance between them known as the HOMO-LUMO gap, or the energy band gap ($E_{(H-L)}$). A compound's density distribution is displayed using HOMO-LUMO, where HOMO denotes the electron-donor zone and LUMO the electron-acceptor region. The HOMO-LUMO data reveal the density distribution of a compound, where the HOMO and LUMO indicate the electron-donor and electron-acceptor regions, respectively [35]. The trend observed in **Fig. S1** illustrates an increase in HOMO energy and a decrease in LUMO energy, typically coinciding with a narrowing of the band gap upon NO_2 gas adsorption, except for the $In_{12}P_{12}$ molecule, which experiences the opposite effect. This alteration leads to a reduced energy band gap in the $X_{12}Y_{12}$-NO_2 system compared to the pristine nanocage due to gas binding.

Global reactivity parameters, like electron affinity (EA), ionization potential (IP), chemical hardness (η), chemical potential (μ), and chemical softness (S),weree computed using the E_{HOMO} and E_{LUMO} data. Density functional theory [36] can be used to implement Parr's function, which was first defined in quantum theory, and Koopman's theorem, as shown in **Table S1**. According to Koopman's theorem, LUMO's negative energy is equal to the electron affinity (EA), but that of HOMO is equal to the ionization potential (IP). The term "ionization potential" (IP) refers to the energy required to liberate a single electron from the outermost shell. A molecule is more reactive when its ionization potential value is low because less energy is required.

Chemical softness and hardness, as well as chemical stability linked to chemical potential, are also correlated with a molecule's E_{HOMO} and E_{LUMO}. The chemical potential (μ), which controls the direction of electron transfer and the movement of charge from low to high electronegativity, can be used to predict an electron's capacity to escape from a stable system [37]. Table S1 shows that all nanocages exhibit negative values across all conditions, indicating the spontaneity and stability of the process [38]. The system with the highest stability is $B_{12}As_{12}$ at -5.0403 eV. The descending order of stability among the nanocages is $B_{12}As_{12} > B_{12}P_{12} > In_{12}P_{12} > In_{12}As_{12}$.

Reactivity also considers chemical softness (S) and chemical hardness (η). Chemical softness describes an atom's capacity to absorb electrons, whereas chemical hardness measures an atom's capacity to supply electrons. Owing to its easier polarizability due to a smaller HOMO and LUMO energy gap, reactivity increases with decreasing chemical hardness values. In other words, a substance will be more reactive as its chemical hardness value decreases and its chemical softness value [38].

The highest E_{gap} in $B_{12}As_{12}$–NO_2 indicates an optimal balance between stability and reactivity, enabling efficient but controlled charge transfer. In contrast, $In_{12}As_{12}$–NO_2 has the smallest gap, which may lead to excessive reactivity that could destabilize the complex. In_{12}-based systems, although softer and with higher EA, may experience excess charge delocalization, leading to less effective binding. $B_{12}As_{12}$–NO_2 has the lowest electron affinity (EA), indicating that it is the most stable system among the others, as it is the least likely to attract additional electrons from any other molecular systems. Less negative μ in $B_{12}As_{12}$–NO_2 suggests it is more electrophilic; thus, it interacts more favorably with the nucleophilic sites in NO_2. Systems with more negative μ (e.g., $In_{12}P_{12}$–NO_2) indicate lower reactivity toward electron donors like NO_2. $B_{12}As_{12}$–NO_2 has moderate hardness and softness, indicating controlled polarizability that supports stable adsorption. $In_{12}As_{12}$–NO_2, despite higher softness (more reactive), may be too unstable to form strong adsorbate–substrate interactions, weakening effective adsorption energy. Thus, $B_{12}As_{12}$–NO_2 is chemically and electronically the most favorable site for strong NO_2 adsorption among the systems studied.

3.4 *Quantum Theory of Atoms in Molecules (QTAIM)*

QTAIM analysis is a method for probing the characteristics of atomic interactions within a molecule [39]. This theory elucidates the structural arrangement of a chemical system by examining the distribution of electron density between pairs of atoms. Bond paths (BP) in QTAIM analysis elucidate the nature of covalent, ionic, and noncovalent bonds within a molecule by tracing lines of elevated electron density that connect bonded atoms. Bond critical points (BCP) serve as focal points of analysis in electron density topology investigations, providing evidence of interatomic connections along bond paths characterized by maximum electron density. **Table S2** presents the topological parameters of electron density (ρ), kinetic energy density (G), Laplacian of the electron density ($\nabla^2\rho$), total energy density (H), potential energy density (V), and the ratio of potential energy density to kinetic energy density (V/G) for both nanocages and NO_2 molecules. The Laplacian and H_{BCP} (Hessian of the Electron Density at the Bond Critical Point) parameters provide insights into molecular interactions. These relationships are governed by specific rules: (i) Positive values of both $\nabla^2\rho$ and H_{BCP} typically indicate weak intermolecular interaction, emphasizing their electrostatic nature (ii) Positive $\nabla^2\rho$ values coupled with negative H_{BCP} values may signify moderate intermolecular interaction, indicating a balance between electrostatic and covalent interactions; and (iii) Negative values of both $\nabla^2\rho$ and H_{BCP} often denote strong intermolecular interaction with covalent characteristics, suggesting significant electron density redistribution and a high degree of stability. Table S2 shows that the $B_{12}As_{12}$-NO_2, $In_{12}As_{12}$-NO_2, and $In_{12}P_{12}$-NO_2 system are partially covalent and have moderate intermolecular interactions. In contrast, $B_{12}P_{12}$-NO_2 system indicate strong intermolecular interaction with covalent characteristics based on both values.

Therefore, the ratio of |V/G | serves as a suitable index to characterize the interaction. For |V/G| values where <1 indicate weak interactions, values between 1 and 2 indicate moderate interactions, while |V/G| > 2 indicates strong interactions [40] [41] [42] [43]. Based on the values in **Table S2**, the entire $X_{12}Y_{12}$-NO_2 system has values less than 1, indicating weak and covalent interactions.

3.5 *Natural Bond Orbital (NBO)*

The NBO analysis provides a convenient method for exploring charge transfer or conjugated interactions in a molecular system, effectively elucidating electrostatic interactions between atoms. The bond strength analysis in computational NBO [44] analysis is based on the second-order perturbation theory, which provides a method to estimate the energies of interactions between filled (donor) Lewis-type NBOs and empty (acceptor) non-Lewis NBOs. These interactions are referred to as "delocalization" corrections for the zeroth-order natural bond orbitals (NBOs). In the NBO analysis, the bond strength is evaluated using the E^2 energy (eq. 10) [45], with elevated values indicating robust interactions and stability between the acceptor and donor orbitals. A larger E^2 value implies a stronger tendency for electron transfer from the donor electron to the acceptor electron, leading to increased electron density delocalization and molecular stability. The second-order perturbation energy can determine intermolecular interaction and charge transfer between Lewis and non-Lewis orbitals, including the energies of donor (i) and acceptor (j) delocalization.

$$E^2 = qi \left(\frac{F(i,j)}{\varepsilon_j - \varepsilon_i}\right) \qquad \text{(Equation 10)}$$

Table S3 shows the interaction between NO_2 molecules and the $X_{12}Y_{12}$ nanocage. In this adsorption system, the $X_{12}Y_{12}$ nanocage functions as the acceptor, while NO_2 gas acts as the donor. The most stable interaction occurs between the O atom in NO_2 as the electron donor and the In atom in the $In_{12}P_{12}$ nanocage as the electron acceptor. The highest Energy Stabilization (E^2) value of 13.24 kcal/mol in this system indicates the strongest and most stable interaction between the acceptor and donor orbitals, which is caused by contact between the Lone Pair (LP) and the Lone Pair Valence (LV) on LP (2) O27 as the donor and LV (1) In1 as the acceptor. **Table S4** presents the values of charge transfer (Q_{CT}) of the nanocage after interaction with NO_2 molecules. Notably, the $In_{12}P_{12}$-NO_2 system demonstrates the greatest charge transfer among the various nanocage systems examined. Specifically, the Mulliken Q_{CT} value is +0.7832 |e|, whereas the NBO Q_{CT} value is 1.364 |e|, indicating the most substantial charge transfer observed compared with the other systems analyzed.

3.6 *Total Density of States (TDOS), Partial Density of States (PDOS), and Overlap Population-based Density of States (OPDOS)*

Frontier Molecular Orbitals (FMO) in Density of States (DOS) analysis validates NO_2 adsorption outcomes, covering chemical orbitals, their interaction roles, and charge transfer. DOS includes total density of states (TDOS), projected density of states (PDOS), and orbital-projected DOS (OPDOS) to examine the Fermi level and occupied/unoccupied orbitals (valence/conduction bands). Using multiwfn software, DOS analysis reveals the effects of nitrogen dioxide adsorption on nanocages. TDOS illustrates the electronic state distribution and occupancy, while PDOS discerns molecular orbital contributions. OPDOS distinguishes bonding interactions (positive, negative, and non-bonding), aiding in understanding NO_2 adsorption bonding mechanisms. Figure S2 shows the adsorption performance based on stability and conductivity, which also shows the bands classified as the valence band and conductivity. In this image, the TDOS, PDOS, and overlap population-based DOS for the B, In, As, P, and NO_2 fragments are represented by the black, red, blue, fuchsia, and green lines, respectively.

Fig. S2 shows that boron and indium are closer to the CB, representing the density of available electronic states at specific energy levels. Higher peaks in $In_{12}P_{12}$ indicate a higher electronic state density.

After adsorbing NO_2, all of the nanocages in **Fig. S2** exhibit a decrease in bandgap energy, as indicated by the plot's $E_{(h-l)}$ value. With a bandgap value of 3.8149 eV that shifts to 2.8689 eV following adsorption, the $B_{12}P_{12}$ nanocage's Projected Density of States (PDOS) are situated at the Highest Occupied Molecular Orbital (HOMO) at -6.9784 eV, as shown in **Fig. S2(b)**. However, **Fig. S2(a)** shows that after adsorb NO_2, the $B_{12}As_{12}$ pure nanocage moved from 3.3035 to 2.9857 eV after adsorp NO2. After adsorption, the band gap changed from the initial band gap of $In_{12}As_{12}$ in **Fig. S2(c)** at 2.1807 eV to 2.006 eV. Lastly, **Fig. S2(d)** displays a band gap of 2.3022 eV and a PDOS at the HOMO of -6.3746 eV, $In_{12}P_{12}$ shifts to 2.3022 eV upon adsorption. Following the adsorption of NO_2 gas, the bandgap energy of all molecules decreases. Since a narrower band gap facilitates simpler excitation of electrons from the VB to the CB, the drop in band gap energy improves conductivity. According to **Eq. 11** (Binet et al., 1994), this has to do with the Boltzmann constant [46]:

$$\sigma \propto \exp\left(-\frac{E_g}{2k_B\mathrm{T}}\right) \qquad \text{(Equation 11)}$$

which, term σ is the electrical conductivity, and k is the Boltzmann constant. Because of the adsorption of NO_2 gas, the adsorption of NO2 gas, resulting in a higher peak intensity.

3.7 *AIMD Simulations*

Ab initio Molecular Dynamics (AIMD) is used for the real-time examination of atomic and molecular motion. Using the Schrödinger equation solution, AIMD tracks particle movement on femtosecond timescales. The principal objective of AIMD analysis is to simulate the $X_{12}Y_{12}$ nanocage's adsorption of NO_2 gas by the X12Y12 nanocage to clarify the adsorbed molecule's final configuration. **Fig. S3** illustrates the results obtained from Ab initio Molecular Dynamics (AIMD) simulations conducted on the $X_{12}Y_{12}$ nanocage, depicting a dynamic temporal evolution. Initially, at t = 0 s, the nanocages display varying distances from the NO_2 gas, ranging from 1.457 to 2.795 Å, with $B_{12}As_{12}$ being the closest to NO_2. Over the 500 femtoseconds (fs) period, both $B_{12}P_{12}$ and $In_{12}As_{12}$ undergo an expansion in distance, while $B_{12}As_{12}$ and $In_{12}P_{12}$ and $In_{12}Sb_{12}$ experience a decrease in distance. By 1000 fs, both $B_{12}P_{12}$ and $In_{12}P_{12}$ distances between NO_2 and the nanocage have increased relative to the initial time, in contrast to $B_{12}As_{12}$ and $In_{12}As_{12}$. Similarly, at 5000 fs, all the systems demonstrate an extension in the distance between the gas and the nanocage.

By increasing the attractive forces and bringing the molecules closer to the surface, proximity causes a robust adsorption in which the molecules firmly bond to the surface. Longer distances, however, highlight the nanocage's amazing femtosecond gas adsorption capability. In conclusion, the $B_{12}As_{12}$-NO_2 system has the shortest length compared to other systems, measuring 1.457 Å at initial time and 1.448 Å at 1000 fs, but it shows a significant distance at the end of 5000 fs. The results show that $B_{12}P_{12}$ has the least electrostatic contact with NO_2 gas, while $B_{12}As_{12}$ has the strongest. The data suggest a greater NO_2 gas adsorption mechanism on the surface of the $B_{12}As_{12}$ nanocage.

3.8 *UV-Vis analysis*

UV-Vis analysis in computational chemistry is used to understand the electronic properties of molecules. This spectrum provides important insights into the electrical structure, characteristics, and possible behaviour of a molecule by showing how electromagnetic radiation or light interacts with its electrons. The aim of UV-Vis analysis is to understand the electronic properties of the $X_{12}Y_{12}$ nanocage material and the adsorbed NO_2 gas molecules and to evaluate the stability and conductivity of the system. This information is crucial for designing and optimizing $X_{12}Y_{12}$ nanocage materials. Molecules absorb light at specific energies, which correspond to electronic transitions within their structure. These absorption events appear in the spectrum as identifiable peaks. The phenomenon becomes particularly interesting when a gas molecule bonds with another, causing changes in the electronic makeup of the resulting system. **Fig. S4** provides a graphical representation of the UV-Visible spectra of $X_{12}Y_{12}$ nanocages, highlighting $B_{12}P_{12}$ as having the highest peak compared to the other nanocages. **Fig. S5** illustrates the spectral changes upon NO_2 adsorption, showing variations in the maximum wavelength for all nanocages. Further analysis in **Table S5** reveals specific wavelength shifts for nanocages $B_{12}As_{12}$, $B_{12}P_{12}$, $In_{12}As_{12}$, and $In_{12}P_{12}$, with values of 736 nm, 450.5 nm, 526.8 nm, and 1546.1 nm, respectively. A thorough comparison of **Fig. S4** and **Fig. S5**, there is a noticeable shift in wavelength for all nanocages. This shift suggests that effective interactions occur between the nanocages and the gas. The $In_{12}P_{12}$-NO_2 system experiences the most notable shift, as evidenced by the absorption band moving to a longer wavelength, indicating a lower energy requirement. Consequently, the $In_{12}P_{12}$-NO_2 configuration proves to be the most advantageous for NO_2 adsorption, demanding less energy, with an oscillator energy of 0.802 eV, resulting from electron excitation from HOMO-1 →HOMO.

3.9 Interaction Region Indicator (IRI) Analysis

Interactions between atoms frequently occur in molecular systems. The IRI analysis method was used to investigate the interaction between gas molecules and nanocage materials. [47]. It provides a comprehensive view of interactions by visualizing both chemical bonds and weak interactions, surpassing the limitations of methods that focus on strong or weak interactions based on color [48]. The color-coded representation of the electron density in the IRI graphics is provided in **Fig. S6**. Important information about the electronic structure and interactions within the molecular system can be found in **Fig. S6(a)–(d)**. The colors in these graphics visually indicate various electron density regions within the molecule: blue, strong interactions between atoms, green denotes weak interactions; and red, steric effects or repulsion. **Fig. S6** illustrates the interaction between the nanocage surface and NO_2 gas. In **Fig. S6(a)**, the red color between atoms B1 and O27 indicates a strong interaction. In **Fig. S6(b)**, the green color between the same atoms indicates a weak interaction. In contrast, in **Fig. S6(c)**, the blue color between atoms In1 and O27 signifies a strong interaction. Simultaneously, **Fig. S6(d)** indicates strong blue-colored interactions between In1 and O27. Blue isosurfaces in the examined nanocages $B_{12}As_{12}$-NO_2, $In_{12}As_{12}$-NO_2, and $In_{12}P_{12}$-NO_2, blue isosurface indicate regions of elevated electron density, implying strength chemical bonding between atoms. Strong interactions between the bonded atoms electrons are suggested by this observation, which suggests stable and well-formed bonds. Conversely, in $B_{12}P_{12}$-NO_2, the presence of green isosurface suggest a comparatively lower electron density, hinting at weaker or less stable interactions between the atoms. Such weak interactions could encompass van der Waals forces or other noncovalent interactions.

3.10 IGMH analysis

The Individual Geometry Minimum Hopping (IGMH) analysis is used to explore the energy landscape of molecules by identifying the lowest energy structures and the pathways connecting them, providing insights into the dynamic behavior of molecules, as well as the pathways (reaction coordinates) connecting $X_{12}Y_{12}$ nanocages and NO_2 molecules. By visualizing the electron density distribution in chemical systems, IGMH can reveal both strong and weak interactions, as well as chemical bond interactions [49], specifically characterizing the interactions between $X_{12}Y_{12}$ nanocages and gases. The analysis uses isosurface of δg to visualize the regions of interaction within the molecule.

The sign function of $(\lambda_2)\rho$, where λ_2 represents the eigenvalues of the electron density Hessian matrix and ρ denotes the corresponding eigenvector, is represented by various colors on the isosurface [50]. When $(\lambda_2)\rho > 0$, , it indicates weak steric interactions. When $(\lambda_2)\rho \approx 0$, it suggests van der Waals interactions. When $(\lambda_2)\rho < 0$, it indicates hydrogen bonding. The figures are depicted with colors representing different characteristics. In **Fig. S7(a),** $B_{12}As_{12}$ shows distinct red and green regions between the nanocage and gas, suggesting significant repulsion and van der Waals interaction. **Fig. S7(b)** displays $B_{12}P_{12}$ in green areas, indicating the existence of van der Waals forces. In **Fig. S7(c)**, the representation of $In_{12}As_{12}$ reveals a combination of green, blue, red, and deep colors between the nanocage and gas, suggesting the occurrence of van der Waals forces and strong intermolecular interactions. **Fig. S7(d)** for $In_{12}P_{12}$ features large green and deep blue areas, indicating forces by van der Waals and significant intermolecular interactions. These findings are further supported by the evidence presented in **Table S5** regarding the value of ρ.

3.11 Electrostatic Potential (ESP) Analysis

The most electron-rich and electron-poor well sites are identified by the ESP (Electrostatic Potential) maps, which can also be used to forecast the potential of charge-dipole, dipole-dipole, and hydrogen bonding interactions. It is useful for understanding the reactivity of polar molecules and predicting their behavior in various chemical reactions [51]. The resulting electrostatic potential field provides information about the interactions between the electrons and the nuclei of the atoms within the molecule. Positive potential regions indicate areas of attraction, where electrons are drawn toward the nucleus, whereas negative potential regions indicate areas of repulsion, where electrons are pushed away from the nucleus [52]. The ESP isosurface maps provide a clear visualization of the total charge distribution and the relative polarity of the $X_{12}Y_{12}$ nanocage and NO_2 gas structure being studied. Moreover, it offers a comprehensive understanding of electrophilicity and nucleophilicity.

The ESP-mapped surfaces depicted in **Fig. S8 (a)-(d)** provide a detailed representation of the electrostatic potential within the molecular system. A detailed analysis of these isosurface reveals distinct characteristics when NO_2 interacts with the nanocage. In **Fig. S8(a),** the NO_2 region bound to $B_{12}As_{12}$ is surrounded by blue (-) isosurface. In contrast, in **Fig. S8(b),** the NO_2 region associated with $B_{12}P_{12}$ displays red (+) isosurface. **Fig. S8(c)** shows that the NO_2 region attached to $In_{12}As_{12}$ is enveloped by blue (−) isosurface, and the NO_2 region in $In_{12}P_{12}$ also exhibits blue (−) isosurface. This suggests that $B_{12}As_{12}$, $In_{12}As_{12}$, and $In_{12}P_{12}$ are influenced by the electron density associated with electron-rich or electron-donating areas of the molecule. These areas are characterized by higher concentrations of negative charges or higher electron densities. Conversely, $B_{12}P_{12}$ presents positive electrostatic potential energy regions, typically associated with electron-poor or electron-accepting areas of the molecule. These areas exhibit reduced electron density or negative charge concentration, which suggests nucleophilic reactivity or the atomic nuclei's repulsion of the proton.

4 Conclusion

Density functional theory calculations using B3LYP/LANL2DZ with D4 dispersion correction have effectively studied the adsorption of NO_2 molecules on fullerene-like $X_{12}Y_{12}$ (X = B, N and Y = In, Sb). The structural characteristics of NO_2 have the lowest distance to $B_{12}As_{12}$, according to the optimum geometry, in line with its lowest adsorption energy among other systems, i.e. 273.3253 kJ/mol. A notable shift in the energy gap of HOMO-LUMO, which results in a decrease in the adsorption energy, suggests that the order of $B_{12}P_{12}$-NO_2 < $In_{12}As_{12}$-NO_2 < $In_{12}P_{12}$-NO_2 < $B_{12}As_{12}$-NO_2 is increasing. The shifted wavelength in the UV-Vis measurement shows that the smallest energy is more advantageous for the adsorption process. Strong intermolecular interaction is suggested by the IRI graphics of the $B_{12}As_{12}$ nanocage, which shows a positive value for $\nabla^2\rho$ and a negative value for H_{BCP}. The deep blue color of the graphics indicates a strong intermolecular interaction between $B_{12}As_{12}$ and NO_2. Based on the value of E^2 from NBO calculation, although $In_{12}P_{12}$–NO_2 has the highest E^2 from a specific donor–acceptor interaction, this does not mean it has the most stable adsorption overall. $B_{12}As_{12}$–NO_2 exhibits the most negative adsorption energy due to a combination of the following: stronger multi-orbital interactions across the surface, favorable electrostatics and reactivity (B and As centers), better binding geometry, and orbital complementarity. Additionally, during the NO_2 adsorption process, variations in the bond length and duration are indicated by the molecular dynamics simulation performed by AIMD. The distance to the $B_{12}As_{12}$ nanocage surface remains the lowest distance between the nanocage and the gas until 5000 fs. All of the abovementioned analyses point to this conclusion, which may help future research on different nanocages and their capacity to adsorb NO_2 molecules. These computational findings highlight $B_{12}As_{12}$ as a highly promising nanocage for NO_2 capture. Future work may include the experimental synthesis of $B_{12}As_{12}$-based nanostructures and gas adsorption measurements (e.g., via FTIR, UV-Vis, or TPD techniques) to validate the computational predictions. Further studies can explore the selectivity toward other environmental pollutants and investigate the regeneration efficiency for potential real-world applications in sensing and air purification.

References

[1] Kumar P., Aishwarya, Srivastava, PK., Pandey MK., Anand A., … Rani M., 2023, Nitrogen dioxide as proxy indicator of air pollution from fossil fuel burning in New Delhi during lockdown phases of COVID-19 pandemic period: impact on weather as revealed by Sentinel-5 precursor (5p) spectrometer sensor, *Environ Dev. Sustain*, pp. 1–12. https://doi.org/10.1007/s10668-023-02977-9

[2] Thurston GD., 2008, Outdoor Air Pollution: Sources, Atmospheric Transport, and Human Health Effects, *International Encyclopedia of Public Health*, H. K. (Kris) Heggenhougen, Ed., Oxford: Academic Press, pp. 700–712. https://doi.org/10.1016/B978-012373960-5.00275-6

[3] Wang M., Li H., Huang S., Qian Y., … Shi L., 2021, Short-term exposure to nitrogen dioxide and mortality: A systematic review and meta-analysis, *Environmental Research*, vol. 202, p. 111766. https://doi.org/10.1016/j.envres.2021.111766

[4] Eum K.-D., Kazemiparkouhi F., Wang B., … Suh H., 2019, Long-term NO_2 exposures and cause-specific mortality in American older adults, *Environment International*, vol. 124, pp. 10–1. https://doi.org/10.1016/j.envint.2018.12.060

[5] Fenech S., & Aquilina NJ., 2020, Trends in ambient ozone, nitrogen dioxide, and particulate matter concentrations over the Maltese Islands and the corresponding health impacts, *Science of The Total Environment*, *700*, 134527. https://doi.org/10.1016/j.scitotenv.2019.134527

[6] Wu HS., Xu XH., Strout DL., & Jiao H., 2005, The structure and stability of B 36 N 36 cages: A computational study, *Journal of Molecular Modeling*, *12*, 1-8. https://doi.org/10.1007/s00894-005-0275-4

[7] Kroto HW., Allaf AW., & Balm SP., 1991, C_{60}: Buckminsterfullerene, *Chem. Rev.*, vol. 91, no. 6, pp. 1213–1235. https://doi.org/10.1021/cr00006a005

[8] Xu SH., Zhang MY., Zhao YY., Chen BG., Zhang J., & Sun CC., 2006, Stability and property of planar (BN) x clusters, *Chemical physics letters*, *423*(1-3), 212-214. https://doi.org/10.1016/j.cplett.2006.03.077

[9] Karimi MSH., & Khovidaki HD., 2019, Studying the surface adsorption of NO_2 gas on $B_{12}N_{12}$ and $B_{12}P_{12}$ nanocages by computational method, *Nano World*, vol. 15, no. 56, pp. 36–43, [Online]. Available: https://donyayenano.ir/article_46127.html

[10] Hussain S., Chatha SAS., Hussain AI., Hussain R., Mehboob MY., … Ayub K., 2020, Designing novel Zn-decorated inorganic $B_{12}P_{12}$ nanoclusters with promising electronic properties: a step forward toward efficient CO_2 sensing materials, *ACS omega*, *5*(25), 15547-15556. https://doi.org/10.1021/acsomega.0c01686

[11] Beheshtian J., Kamfiroozi M., Bagheri Z., & Peyghan AA., 2012, $B_{12}N_{12}$ nano-cage as potential sensor for NO2 detection, *Chinese Journal of Chemical Physics*, *25*(1), 60 https://doi.org/10.1088/1674-0068/25/01/60-64

[12] Beheshtian J., Kamfiroozi M., Bagheri Z., & Ahmadi A., 2012, Theoretical study of hydrogen adsorption on the B12P12 fullerene-like nanocluster, *Computational materials science*, *54*, 115-118. https://doi.org/10.1016/j.commatsci.2011.09.039

[13] Ektarawong A., Simak SI., & Alling B., 2017, First-principles prediction of stabilities and instabilities of compounds and alloys in the ternary B-As-P system, *Physical Review B*, *96*(2), 024202. https://doi.org/10.1103/PhysRevB.96.024202

[14] Neese F., 2012, The ORCA program system, *Wiley Interdisciplinary Reviews: Computational Molecular Science*, *2*(1), 73-78. https://doi.org/10.1002/wcms.81

[15] Hertwig RH., & Koch W., 1997, On the parameterization of the local correlation functional, What is Becke-3-LYP?, *Chemical Physics Letters*, *268*(5-6), 345-351. https://doi.org/10.1016/S0009-2614(97)00207-8

[16] Becke AD., 1988, Density-functional exchange-energy approximation with correct asymptotic behavior, *Physical review A*, *38*(6), 3098. https://doi.org/10.1103/physreva.38.3098

[17] Lee C., Yang W., & Parr RG., 1988, Development of the Colle-Salvetti correlation-energy formula into a functional of the electron density, *Physical review B*, *37*(2), 785. https://doi.org/10.1103/physrevb.37.785

[18] Becke AD., 1993, A new mixing of Hartree-Fock and local density-functional theories, *Journal of chemical Physics*, *98*(2), 1372-1377. https://doi.org/10.1063/1.464304

[19] Check CE., Faust TO., Bailey JM., Wright BJ., Gilbert TM., & Sunderlin LS., 2001, Addition of polarization and diffuse functions to the LANL2DZ basis set for p-block elements, *The Journal of Physical Chemistry A*, *105*(34), 8111-8116. https://doi.org/10.1021/jp011945l

[20] Caldeweyher E., Mewes JM., Ehlert S., & Grimme S., 2020, Extension and evaluation of the D4 London-dispersion model for periodic systems, *Physical Chemistry Chemical Physics*, *22*(16), 8499-8512. https://doi.org/10.1039/D0CP00502A

[21] Caldeweyher E., Ehlert S., Hansen A., Neugebauer H., Spicher S., Bannwarth C., & Grimme S., 2019, A generally applicable atomic-charge dependent London dispersion correction, *The Journal of chemical physics*, *150*(15). https://doi.org/10.1063/1.5090222

[22] Hanwell MD., Curtis DE., Lonie DC., Vandermeersch T., Zurek E., & Hutchison GR., 2012, Capillary surfaces with free boundary in a wedge, *J. Cheminform.*, vol. 262. https://doi.org/10.1016/j.aim.2014.05.019

[23] Qian, 2005, Electronic Supplementary Information, *Acad. Version*, vol. 63, no. c, pp. 1–13.

[24] Tian L., and Chen F., 2012, J. Comput, vol. 33, pp. 580–592.

[25] Humphrey W., Dalke A., & Schulten K., 1996, VMD: visual molecular dynamics, *Journal of molecular graphics*, *14*(1), 33-38. https://doi.org/10.1016/0263-7855(96)00018-5

[26] Badran HM., Eid KM., Baskoutas S., & Ammar HY., 2022, $Mg_{12}O_{12}$ and $Be_{12}O_{12}$ nanocages as sorbents and sensors for H2S and SO_2 gases: A theoretical approach, *Nanomaterials*, *12*(10), 1757. https://doi.org/10.3390/nano12101757

[27] Choir AA., Amelia SR., Martoprawiro MA., Kusumawati Y., & Ivansyah AL., 2024, Insight into the adsorption properties of CO_2 and H_2 gas on the $B_{12}Y_{12}$ (YN, P, As, Sb) nanocages from host-guest interaction perspective, *International Journal of Hydrogen Energy*, *53*, 780-791. https://doi.org/10.1016/j.ijhydene.2023.12.030

[28] Neto VDOS., Raulino GSC., Paulo de Tarso CF., Araújo-Silva MA., & do Nascimento RF., 2013, Equilibrium and kinetic studies in adsorption of toxic metal ions for wastewater treatment, *viewpoints*, *7*(8).

[29] Hussain S., Shahid Chatha SA., Hussain AI., Hussain R., Mehboob MY., … Ayub K., 2020, Designing novel Zn-decorated inorganic $B_{12}P_{12}$ nanoclusters with promising electronic properties: a step forward toward efficient CO_2 sensing materials, *ACS omega*, *5*(25), 15547-15556. https://doi.org/10.1021/acsomega.0c01686

[30] Karthikaiselvi R., & Subhashini S., 2014, Study of adsorption properties and inhibition of mild steel corrosion in hydrochloric acid media by water soluble composite poly (vinyl alcohol-o-methoxy aniline), *Journal of the Association of Arab Universities for Basic and Applied Sciences*, *16*, 74-82. https://doi.org/10.1016/j.jaubas.2013.06.002

[31] Adjal C., Timón V., Guechtouli N., Boussassi R., Hammoutène D., & Senent ML., 2023, The role of water in the adsorption of nitro-organic pollutants on activated carbon, *The Journal of Physical Chemistry A*, *127*(39), 8146-8158. https://doi.org/10.1021/acs.jpca.3c03877

[32] Zhang H., Qin H., Wang X., Pan Y., He P., Wu J., & Fan W., 2023, Revealing the influence of oxygen-containing functional groups on mercury adsorption via density functional theory and multiple linear regression analysis, *Fuel*, *335*, 127040. https://doi.org/10.1016/j.fuel.2022.127040

[33] Huber F., Berwanger J., Polesya S., Mankovsky S., Ebert H., & Giessibl FJ., 2019, Chemical bond formation showing a transition from physisorption to chemisorption, *Science*, *366*(6462), 235-238. https://www.science.org/doi/10.1126/science.aay3444

[34] Shen F., Liu J., Zhang Z., Dong Y., & Gu C., 2018, Density functional study of hydrogen sulfide adsorption mechanism on activated carbon, *Fuel processing technology*, *171*, 258-264. https://doi.org/10.1016/j.fuproc.2017.11.026

[35] Miar M., Shiroudi A., Pourshamsian K., Oliaey AR., & Hatamjafari F., 2021, Theoretical investigations on the HOMO–LUMO gap and global reactivity descriptor studies, natural bond orbital, and nucleus-independent chemical shifts analyses of 3-phenylbenzo [d] thiazole-2 (3 H)-imine and its para-substituted derivatives: Solvent and substituent effects, *Journal of Chemical Research*, *45*(1-2), 147-158. https://doi.org/10.1177/1747519820932091

[36] Nazarov VU., 2021, Ionization potential of extended systems: Validity of Koopmans' theorem in the Hartree-Fock theory and invalidity of the IP-theorem in density functional theory, [Online]. Available: http://arxiv.org/abs/2104.07882

[37] Sessa F., & Rahm M., 2022, Electronegativity equilibration, *The Journal of Physical Chemistry A*, *126*(32), 5472-5482. https://doi.org/10.1021/acs.jpca.2c03814

[38] Qing L., 1997, Supporting Information Supporting Information, *Aldenderfer, Mark S., Craig, Nathan M., Speak. Robert Jeff, Popelka-Filcoff, Rachel S.*, vol. 2, no. 1, pp. 1–5.

[39] Tarika JD., Dexlin XD., Rathika A., Jayanthi DD., & Beaula TJ., 2022, Computational

insights on charge transfer and non-covalent interactions of antibacterial compound 4-dimethylaminopyridinium pyridine-2-carboxylate pentahydrate, *Journal of Molecular Structure*, *1256*, 132525. https://doi.org/10.1016/j.molstruc.2022.132525
[40] Rozas I., Alkorta I., & Elguero J., 2000, Behavior of ylides containing N, O, and C atoms as hydrogen bond acceptors, *Journal of the American Chemical Society*, *122*(45), 11154-11161. https://doi.org/10.1021/ja0017864
[41] Koch U., & Popelier PL., 1995, Characterization of CHO hydrogen bonds on the basis of the charge density, *The Journal of Physical Chemistry*, *99*(24), 9747-9754. https://doi/org/10.1021/j100024a016
[42] Siahaan P., Sasongko NA., Lusiana RA., Prasasty VD., & Martoprawiro MA., 2021, The validation of molecular interaction among dimer chitosan with urea and creatinine using density functional theory: In application for hemodyalisis membrane, *International Journal of Biological Macromolecules*, *168*, 339-349. https://doi.org/10.1016/j.ijbiomac.2020.12.052
[43] Rezaei-Sameti M., & Zarei PNBO., 2018, NBO, AIM, HOMO–LUMO and thermodynamic investigation of the nitrate ion adsorption on the surface of pristine, Al and Ga doped BNNTs: A DFT study, *Adsorption*, *24*(8), 757-767. https://doi.org/10.1007/s10450-018-9977-7
[44] Weinhold F., & Landis CR., 2005, *Valency and bonding: a natural bond orbital donor-acceptor perspective*, Cambridge University Press. https://doi.org/10.1017/CBO9780511614569
[45] Ghosh S., Chopra P., & Wategaonkar S., 2020, C–H··· S Interaction exhibits all the characteristics of conventional hydrogen bond, *Physical Chemistry Chemical Physics*, *22*(31), 17482-17493. https://doi.org/10.1039/d0cp01508c
[46] Binet L., Gourier D., & Minot C., 1994, Relation between electron band structure and magnetic bistability of conduction electrons in β-Ga2O3, *Journal of Solid State Chemistry*, *113*(2), 420-433. https://doi.org/10.1006/jssc.1994.1390
[47] Sravanthi R., Mahalakshmi S., Vetrivelan V., Irfan A., & Muthu S., 2023, Absorption wavelength (TD-DFT) and adsorption of metal chalcogen clusters with methyl nicotinate: Structural, electronic, IRI, SERS, pharmacological and antiviral studies (HIV and omicron, *Heliyon*, *9*(5). https://doi.org/10.1016/j.heliyon.2023.e16066
[48] Lu T., & Chen Q., 2021, Interaction region indicator: a simple real space function clearly revealing both chemical bonds and weak interactions, *Chemistry-Methods*, *1*(5), 231-239. https://doi.org/10.1002/cmtd.202100007
[49] Lu T., & Chen Q., 2021, Independent gradient model based on Hirshfeld partition (IGMH): A new method for visual study of interactions in chemical systems, *ChemRxiv*. https://doi.org/10.26434/chemrxiv-2021-628vh-v2
[50] Lu T, Chen Q., and Lu OT., 1822, Independent gradient model based on Hirshfeld partition (IGMH): A new method for visual study of interactions in chemical systems, pp. 1–30, [Online]. Available: http://www.keinsci.com
[51] Gautam BPS., Srivastava M., Prasad RL., & Yadav RA., 2014, Synthesis, characterization and quantum chemical investigation of molecular structure and vibrational spectra of 2, 5-dichloro-3, 6-bis-(methylamino) 1, 4-benzoquinone, *Spectrochimica Acta Part A: Molecular and Biomolecular Spectroscopy*, *129*, 241-254. https://doi.org/10.1016/j.saa.2014.02.082
[52] Kühne TD., Iannuzzi M., Del Ben M., Rybkin VV., Seewald P., … Hutter J., 2020, CP2K: An electronic structure and molecular dynamics software package-Quickstep: Efficient and accurate electronic structure calculations, *The Journal of Chemical Physics*, *152*(19). https://doi.org/10.1063/5.0007045